Two-photon Raman transition channels of NaCs predicted from *ab initio* calculations

Jingbo Wei,[1] Peng Li,[1,3,*] Jizhou Wu,[1,3] Vladimir Sovkov,[1,4] Wenliang Liu,[1,3] Yuqing Li,[1,3] Yongming Fu,[1,3] Feng Xie,[2] and Jie Ma[1,3,†]

[1]*School of Physics and Electronic Engineering, State Key Laboratory of Quantum Optics and Quantum Optics Devices, Institute of Laser Spectroscopy, Shanxi University, Taiyuan 030006, China*

[2]*Institute of Nuclear and New Energy Technology, Collaborative Innovation Center of Advanced Nuclear Energy Technology, Key Laboratory of Advanced Reactor Engineering and Safety of Ministry of Education, Tsinghua University, Beijing 100084, China*

[3]*Collaborative Innovation Center of Extreme Optics, Shanxi University, Taiyuan 030006, China*

[4]*St. Petersburg State University, 7/9 Universitetskaya nab., St. Petersburg 199034, Russia*

(Received 17 February 2022; accepted 2 June 2022; published 22 June 2022)

Obtaining effective spontaneous radiative transition channels is a fundamental topic in the preparation of ultracold rovibrational ground states of molecules. Herein, the ranges of prospective transition channels in the NaCs dimer are predicted via exploring the complex energy level structure and transition properties. The potential energy curves of Λ-S states and Ω states, spectroscopy constants, absolute energies of bound states, and transition information (Frank-Condon factors, lifetimes, transition dipole moments) have been researched. With this purpose, the results of our experiment on binding energies of the $b^3\Pi_0{}^+$ rovibrational states are analyzed; the transition from the higher (photoassociated) $^1\Pi$ state to the ground $X^1\Sigma^+$ state is discussed. The wavelengths of the two lasers are predicted as 622.8-656.7 nm and 896.3-969.8 nm with the $B^1\Pi_1$ and $c^3\Sigma_1^+$ states, respectively, for the stimulated raman adiabatic passage method.

DOI: 10.1103/PhysRevA.105.063322

I. INTRODUCTION

Ultracold molecules have rich internal structure and symmetry, including vibrational, rotational, and hyperfine structure. Particularly, ultracold heteronuclear polar molecules have large permanent electric dipole moments, long-life fine energy level structures, and long-range dipole-dipole interactions [1–3], which make it easy to realize field manipulations, obtain an internal state with a longer coherent time, and promote the production of novel quantum states. Therefore, polar molecules are applied to the preparation of dipole crystals [4], quantum computation [5,6], quantum simulation [7,8] and quantum chemistry research [9,10]. However, the realization of these prospects has been hindered by sticky collisions between molecules, such that it limits the lifetime of molecular samples [11,12], affects the ability to cool molecular collisions to high phase space densities [13], and destroys Feshbach resonance [14]. By loading the molecule into the optical lattice potential, the collision reaction can be effectively suppressed and the lifetime of the molecular sample can be extended [15].

NaCs molecule has the second largest electric dipole moment among all the heteronuclear alkali diatomic molecules [16], strong spin-orbit coupling, chemical reaction (NaCs + NaCs $\rightarrow$ $Na_2 + Cs_2$) endothermic as high as 236.75 cm^{-1}, being the most stable of alkali metal polar molecules [17]. Such properties make it an ideal system for realizing ultracold molecules.

Some theoretical [18–23] and experimental [16], [24–45] studies have been carried out on NaCs molecules during the recent decades. In terms of theoretical calculations, Igel-Mann *et al.* [18] investigated NaCs molecules based on the pseudopotential and configuration interaction (CI) methods, obtained the spectroscopic constants of the ground state of NaCs molecules. The states $^{1,3}\Sigma^+$, $^{1,3}\Pi$ and $^{1,3}\Delta$ were described by Korek *et al.* [19] based on nonempirical pseudopotential and parametrized l-dependent polarization potentials via full configuration interaction calculations. After that, the potential energy curves (PECs) were investigated by considering the spin-orbit coupling (SOC) effect from the same team [21]. Adiabatic and diabatic potential energy curves and dipole moments were calculated by Mabrouk and Berriche using the same method [23]. Dardouri *et al.* [22] calculated the PECs and vibrational energy levels of NaX (X = Rb, Cs), with the core-potentials and full valence configuration.

There are comparatively many studies of experimental aspects. By using the photoassociation (PA) method, the ultracold NaCs molecules were created by Bigelow and his colleagues for the first time [35]. Haimberger's group have reported that the laser-cooled Na and Cs atomic vapors begin to form the translational cold NaCs molecules [36]; shortly after, they reported the formation process of the ground-state NaCs molecules by the PA approach [27]. Then, PA spectroscopy of ultracold NaCs molecules formed in a magneto-optical trap have been obtained by the same team and they detected the long-range state of $\Omega = 2$ [37]. The $X^1\Sigma^+$, $a^3\Sigma^+$, and

*Corresponding author: lip@sxu.edu.cn
†Corresponding author: mj@sxu.edu.cn

$B^1\Pi$ states have been investigated by Docenko *et al.* [26] and Zaharova *et al.* [38]. The $5^3\Pi_0$ and $1(a)^3\Sigma^+$ states were studied by Ashman *et al.* [39]. Several deeply bound vibrational quantum states of the NaCs ground electronic state were labeled by Zabawa *et al.* [40], after that, the ultracold $X^1\Sigma^+$ ($v'' = 0$) NaCs molecules were formed via coupling PA channels by them [41]. Laser-induced fluorescence (LIF) spectra $(4)^1\Sigma^+ \rightarrow A^1\Sigma^+$-$b^3\Pi$ and collisionally enhanced $A^1\Sigma^+$-$b^3\Pi \rightarrow X^1\Sigma^+$ LIF spectra measured by Zabawa *et al.* [28] via Fourier transform spectrometer, and they provided about 1160 term values of the *e*-symmetry rovibronic levels of the fully mixed $A^1\Sigma^+$ and $b^3\Pi$ states of a NaCs molecule. In 2017, the NaCs $12(0^+)$ $[7^1\Sigma^+]$ state was investigated by Faust *et al.* [42], the $11(0^+)$ and $12(0^+)$ electronic states of the NaCs molecule were analyzed, and a theoretical model describing the experiment was suggested. In 2018, two cold atoms were combined into an excited state of NaCs molecule using optical tweezers [43]. This brought the preparation of the NaCs molecule vibrational ground state one step closer. Recently, a rovibrational ground state NaCs molecule created in an optical tweezer by THE Kang-Kuen Ni [59] group was reported.

Since 2016, our group has been devoted to the efficient preparation of rovibrational ground state NaCs molecules both experimentally and theoretically, achieved a series of advances in the preparation, spectroscopy, and theoretical simulation of ultracold NaCs molecules [31,32,44,45]. The hyperfine structures of the excited $c^3\Sigma^+$ and $b^3\Pi$ states of ultracold NaCs molecules near the $3S_{1/2} + 6P_{3/2}$ dissociation limit were studied via high-resolution trap-loss spectroscopy technology.

In this paper, the PECs of NaCs molecule are calculated, the spectroscopy constants of each electronic state and information on the excited to ground state transitions are obtained. The calculated energy values of each bound state with the PECs including SOC were used to analyze the spectroscopy obtained in the experiment and explain the mixed states of $A^1\Sigma^+$ and $b^3\Pi$. In addition, we predicted the wavelength ranges of two lasers in the two-photon Raman transition for the $B^1\Pi_1$ and $c^3\Sigma_1^+$ states when preparing the NaCs molecules in the absolute rovibrational ground state by the stimulated raman adiabatic passage (STIRAP) method.

II. COMPUTATIONAL DETAILS

The electronic structure is calculated for 16 singlet and triplet states containing $^{1,3}\Sigma^+$, $^{1,3}\Pi$ and $^{1,3}\Delta$ components under the first four lowest dissociation asymptotes and 19 Ω electronic states after considering the SOC effect in NaCs. All single single-point energy calculations are performed by the averaged complete active space self-consistent field (SA-CASSCF) [46,47] and multireference configuration interaction (MRCI) [48–50] method. Higher-order CI terms are corrected by the Davidson correction method. Scalar relativistic effects are embedded through the pseudopotential basis set of def2-QZVPPD [51]. We applied the counterpoise correction to evaluate the basis set superposition error (BSSE) in the interaction energy to be around $1.13\,\mathrm{cm}^{-1}$ at the equilibrium internuclear, and the values of BSSE decreases with increasing internuclear distance ($R_{\mathrm{Na-Cs}} = 10$Å, BSSE $\approx 0.12\,\mathrm{cm}^{-1}$). Therefore, BSSE is not considered in the calculation.

For both CASSCF and MRCI calculations, the orbitals $1s2s$ for Na and $5s$ for Cs atoms are placed into the core orbitals. The effective active space holds the orbitals $6s6p5d6d7s$ for Cs and $3s3p4s$ for Na. In the selection of the activity space, extensive testing has been done, which is detailed in the Supplemental Material [52]. The SOC [53] is included in the MRCI calculation of electronic properties, producing a giant spin-orbit-induced splitting through the effective core potential (ECP) spin-orbit operator. The entire SO matrix elements are calculated and diagonalized. The calculations of NaCs are performed in the C_{2v} point group and carried out with the MOLPRO 2015 [54,55] program.

Based on computed Λ-*S* and Ω PECs, equilibrium internuclear distance R_e, excitation energy T_e, vibrational constants ω_e and $\omega_e x_e$, and equilibrium rotation constant B_e are evaluated for all electronic states. Meanwhile, energy levels, rotational, and centrifugal distortion constants for the vibrational levels of the low-lying electronic states of NaCs are obtained by numerically solving the one-dimensional Schrödinger equation of nuclear motion, with the aid of the LEVEL [56] program package. Besides, the Franck-Condon factors, Einstein coefficients and radiative lifetimes have also been determined.

The Einstein coefficient for a transition from an initial-state level (v', J') into a final-state level (v'', J'') in units s^{-1} is

$$A(v', J', v'', J'') = 3.1361891 \times 10^{-7} \frac{S(J', J'')}{2J' + 1} |T_{v'J'} - T_{v''J''}|^3 \times |\langle \Psi_{v',J'} | M(r) | \Psi_{v'',J''} \rangle|^2, \quad (1)$$

and the radiation lifetime of the upper-state (v', J') level decaying into the bunch of the lower-state (v'', J'') levels in units s is

$$\tau_{v'J'} = \frac{1}{\sum_{v''J''} A(v', J', v'', J'')}, \quad (2)$$

where $M(r)$ is the dipole moment (or transition dipole) function in units Debye, $S(J', J'')$ is the Hönl-London rotational intensity factor, $\Psi_{v',J'}$ and $\Psi_{v'',J''}$ are the unit-normalized initial and final state radial wave functions, $T_{v'J'}$ and $T_{v''J''}$ are the corresponding term values.

The binding energies are obtained by subtracting the energy of different vibration-rotation states from the dissociation asymptote energy.

III. RESULTS AND DISCUSSION

A. Spectroscopic constants and dipole moments of Λ-*S* states

The 14 Λ-*S* states of the NaCs molecule corresponding to four lowest dissociation asymptotes Na ($3S$) + Cs ($6S$), Na ($3S$) + Cs ($6P$), Na ($3S$) + Cs ($5D$) and Na ($3S$) + Cs ($6S$) have been investigated at the MRCI + Q level of theory. The PECs are shown for $^{1,3}\Sigma^+$, $^{1,3}\Pi$ and $^{1,3}\Delta$ states in Fig. 1. The correlation effects of $5d^{10}$ and $6d^{10}$ electrons of Cs are considered in the calculation.

The inset in Fig. 1 displays the avoiding crossing of the $E^1\Sigma^+$ and $(1)^1\Delta$ states as the enlargement of the red circle. This is caused by a strong coupling effect. It can be seen from

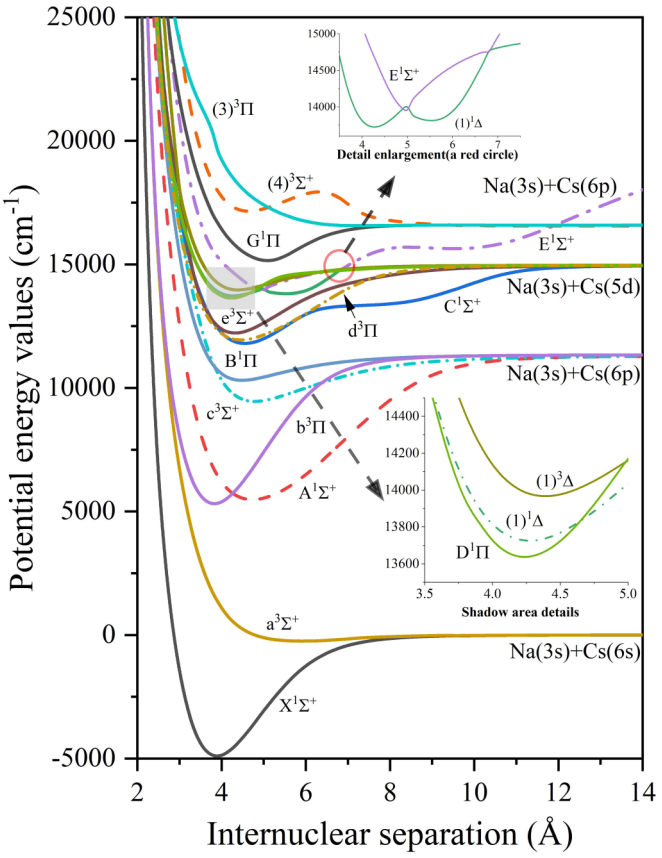

FIG. 1. PECs of 14 Λ-*S* states of NaCs molecule.

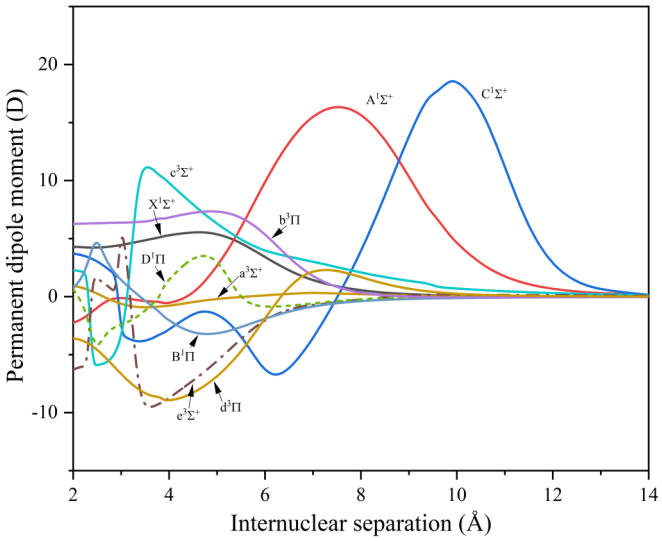

FIG. 2. Permanent dipole moments of NaCs molecule.

the shadowed area that there is a large wave function overlap of the bound states $D^1\Pi$, $(1)^1\Delta$ and $(1)^3\Delta$. The $C^1\Sigma^+$, $E^1\Sigma^+$ and $(4)^3\Sigma^+$ states have double potential wells.

In order to ensure the rationality of the value of equilibrium internuclear distance R_e, in the test, we have very intensive fetching around the equilibrium point. Comparison of the calculated values of spectroscopic constants with other theoretical calculations and experimental results is shown in Table I.

Comparing with the spectroscopic constants calculated via the Full valence configuration interaction approach by Korek *et al.* [19], the range of numerical difference for R_e, T_e, ω_e, $\omega_e x_e$, and B_e are 0.02–0.25 Å, 10.0–206.0 cm^{-1}, 0.00–8.88 cm^{-1}, 0.04–1.99 cm^{-1}, and 0.004–0.07 cm^{-1}, respectively. Meanwhile, the differences between the MRCI and full configuration interaction (FCI) [23] results for the same quantities are 0.03–0.20 Å, 0.0–246.2 cm^{-1}, 0.22–8.75 cm^{-1}, 0.01–1.90 cm^{-1}, 0.001–0.004 cm^{-1}, respectively. At the same time, data with relatively large differences but within a reasonable range is included in the comparison results of two theoretical calculations: the discrepancies of T_e are ∼2.2%–2.0% for $^1\Delta$ and $\sim 2.1\% - 2.0\%$ for $^3\Delta$; the values of $\delta R_e = 0.82$ Å for $(3)^3\Pi$ by Mabrouk *et al.* [23] and $\delta R_e = 0.80$ Å for $G^1\Pi$ by Korek *et al.* [19]. Comparing the experiment by Diemer *et al.* [25], the differences R_e of the ground state are 0.0375, 0.0466, and 0.0376 Å for MRCI, FCI and full valence CI.

In summary, the calculated results of MRCI are overall slightly larger compared to the existing theoretical calculated values, and there is good consistency at the first three dissociation limits. Particularly, the results of the ground state

TABLE I. Spectroscopic constants of the NaCs molecule.

State	R_e (Å)	T_e (cm^{-1})	ω_e (cm^{-1})	$\omega_e x_e$ (cm^{-1})	B_e (cm^{-1})	Ref.
$X^1\Sigma^+$	3.888	0	98.20	0.35	0.0569	This work
	3.805					CI [22]
	3.804		98.04	0.38	0.0594	CI [23]
	3.851					Expt. [25]
	3.690				0.0631	Expt. [28]
	3.850		99.00			Expt. [24]
	3.813		99.97		0.0592	CI [19]
	3.769		101.90		0.0605	CI [21]
	3.809					CI [20]
	3.830		98.00			CI [18]
$a^3\Sigma^+$	5.911	4660	20.44	0.30	0.0246	This work
	5.735	4779	22.30	2.20	0.0262	CI [23]
	5.766	4695				CI [22]
	5.745	−217				Expt. [25]

TABLE I. (*Continued.*)

State	R_e (Å)	T_e (cm^{-1})	ω_e (cm^{-1})	$\omega_e x_e$ (cm^{-1})	B_e (cm^{-1})	Ref.
$A^1\Sigma^+$	4.731	10382	56.84	0.04	0.0384	This work
	4.620	10527	57.79	0.16	0.0404	CI [23]
	4.610	10473				CI [22]
	4.650					Expt. [28]
	4.480	10511	105.08		0.0428	CI [19]
$b^3\Pi$	3.833	10212	96.43	0.25	0.0587	This work
	3.757	10244				CI [22]
	3.735	10266	96.21	0.28	0.0617	CI [23]
	3.780	10236				Expt. [28]
	3.737	10277	99.28		0.0616	CI [19]
$c^3\Sigma^+$	4.783	14357	53.52	0.48	0.0376	This work
	4.640	14603	53.85	0.49	0.0399	CI [23]
	4.660	14548				CI [22]
	4.610	14538	55.50		0.0405	CI [19]
$B^1\Pi$	4.482	15213	51.08	0.72	0.0428	This work
	4.390	15336				CI [22]
	4.360	15393	54.16	0.85	0.0452	CI [23]
	4.381	15341	53.75		0.0448	CI [19]
$C^1\Sigma^+$	4.552	16705	62.68	0.22	0.0415	This work
	4.470	16656				CI [22]
	4.466	16736	62.24	0.25	0.0431	CI [23]
	4.417	16665	91.60		0.0441	CI [19]
$d^3\Pi$	4.453	16847	56.51	0.25	0.0434	This work
	4.394	16738				CI [22]
	4.365	16810	55.57	0.28	0.0451	CI [23]
	4.398	16737	56.51		0.0445	CI [19]
$e^3\Sigma^+$	4.317	17125	67.04	0.34	0.0462	This work
	4.275	16994	67.68	0.50	0.0470	CI [23]
	4.277	16933				CI [22]
	4.297	16919	67.43		0.0466	CI [19]
$D^1\Pi$	4.235	18537	71.01	0.55	0.0480	This work
	4.213	18453				CI [22]
	4.206	18470	66.69	0.37	0.0486	CI [23]
	4.205	18470	69.34		0.0486	CI [19]
$E^1\Sigma^+$	4.987	18827	109.29	4.41	0.0348	This work
	4.789	18996				CI [22]
	5.286	18777	41.52	0.02		CI [23]
	4.536	19068	139.98		0.0418	CI [19]
	5.155	18973	40.80		0.0323	CI [21]
$G^1\Pi$	5.098	20057	62.29	0.43	0.0331	This work
	6.380	21516				CI [22]
	4.894	20052	64.33	0.01	0.0359	CI [23]
	5.895	20047	65.68		0.0359	CI [19]
$(3)^3\Pi$	7.259	21471	11.88	1.24	0.0164	This work
	4.880	19957				CI [22]
	6.444	21618	25.45	−0.03	0.0207	CI [23]
$^1\Delta$	4.270	18627	50.10	1.99	0.0472	This work
	4.227	18147				CI [22]
	4.185	18208	58.85	0.22	0.0491	CI [23]
	4.215	18252	58.98		0.0484	CI [19]
$^3\Delta$	4.387	18869	54.22	0.70	0.0447	This work
	4.339	18405				CI [22]
	4.302	18465	54.91	0.80	0.4649	CI [23]
	4.342	18490	53.00		0.0456	CI [19]

TABLE II. Franck-Condon factors (FCFs) for $Z\,(v', J'=0)$ - $X^1\Sigma^+\,(v'', J''=0)$ ($Z = A^1\Sigma^+, C^1\Sigma^+, B^1\Pi, D^1\Pi$) (Numbers in parentheses indicate the power of 10).

	v''	$v'=0$	$v'=1$	$v'=2$	$v'=3$	$v'=4$	$v'=5$
$A^1\Sigma^+$-$X^1\Sigma^+$	0	3.94[−7]	4.77[−6]	2.98[−5]	1.27[−4]	4.19[−4]	1.13[−3]
	1	6.58[−6]	6.96[−5]	3.77[−4]	1.39[−3]	3.90[−3]	8.92[−3]
	2	5.43[−5]	4.95[−4]	2.29[−3]	7.10[−3]	1.66[−2]	3.10[−2]
	3	2.94[−4]	2.27[−3]	8.77[−3]	2.24[−2]	4.18[−2]	6.04[−2]
	4	1.18[−3]	7.56[−3]	2.37[−2]	4.77[−2]	6.74[−2]	6.80[−2]
	5	3.70[−3]	1.93[−2]	4.76[−2]	7.11[−2]	6.78[−2]	3.75[−2]
$C^1\Sigma^+$-$X^1\Sigma^+$	0	7.81[−5]	6.59[−4]	2.85[−3]	8.42[−3]	1.91[−2]	3.54[−2]
	1	8.12[−4]	5.48[−3]	1.85[−2]	4.17[−2]	6.95[−2]	9.05[−2]
	2	4.16[−3]	2.17[−2]	5.46[−2]	8.67[−2]	9.37[−2]	6.79[−2]
	3	1.40[−2]	5.38[−2]	9.34[−2]	9.03[−2]	4.49[−2]	4.77[−3]
	4	3.45[−2]	9.21[−2]	9.64[−2]	3.86[−2]	2.52[−4]	2.19[−2]
	5	6.66[−2]	1.12[−1]	5.26[−2]	2.49[−4]	2.98[−2]	5.65[−2]
$B^1\Pi$-$X^1\Sigma^+$	0	6.75[−4]	3.85[−3]	1.16[−2]	2.46[−2]	4.15[−2]	5.92[−2]
	1	4.81[−3]	2.12[−2]	4.83[−2]	7.52[−2]	8.91[−2]	8.45[−2]
	2	1.73[−2]	5.64[−2]	9.01[−2]	9.03[−2]	5.93[−2]	2.22[−2]
	3	4.18[−2]	9.44[−2]	9.26[−2]	4.32[−2]	4.23[−3]	5.30[−3]
	4	7.62[−2]	1.08[−1]	4.85[−2]	1.23[−3]	1.68[−2]	4.60[−2]
	5	1.12[−1]	8.47[−2]	5.45[−3]	1.89[−2]	5.26[−2]	3.59[−2]
$D^1\Pi$-$X^1\Sigma^+$	0	5.62[−2]	1.58[−1]	2.27[−1]	2.20[−1]	1.62[−1]	9.66[−2]
	1	1.63[−1]	1.95[−1]	6.36[−2]	4.12[−4]	6.08[−2]	1.35[−1]
	2	2.38[−1]	6.14[−2]	1.87[−2]	1.12[−1]	7.50[−2]	3.80[−3]
	3	2.29[−1]	1.64[−3]	1.17[−1]	3.99[−2]	1.22[−2]	8.50[−2]
	4	1.62[−1]	7.79[−2]	7.12[−2]	1.59[−2]	9.02[−2]	1.86[−2]
	5	9.01[−2]	1.57[−1]	5.96[−4]	9.58[−2]	1.52[−2]	3.82[−2]

are closer to experimental data than others. The permanent electric dipole moments of the 10 Λ-S states are obtained by MRCI method and displayed in Fig. 2.

B. Transition properties and radiative lifetimes of Λ-S states

The transition dipole moments (TDMs) are obtained simultaneously with the PECs calculated at the MRCI level.

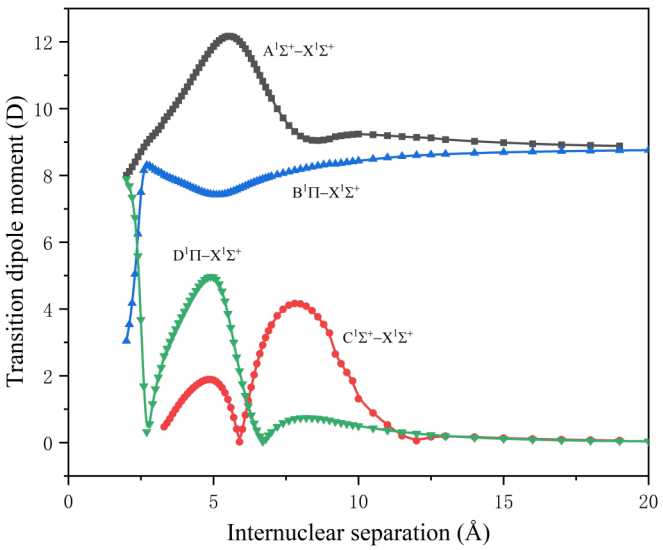

FIG. 3. Absolute values of TDMs of $A^1\Sigma^+, C^1\Sigma^+, B^1\Pi, D^1\Pi$ to $X^1\Sigma^+$.

The absolute values of TDMs of $A^1\Sigma^+$-$X^1\Sigma^+$, $C^1\Sigma^+$-$X^1\Sigma^+$, $B^1\Pi$-$X^1\Sigma^+$ and $D^1\Pi$-$X^1\Sigma^+$ pairs are shown in Fig. 3. The TDMs between other electronic states are placed in Tables S1-S2. Overall, the transition probabilities of $A^1\Sigma^+$-$X^1\Sigma^+$ and $B^1\Pi$-$X^1\Sigma^+$ are greater than of $C^1\Sigma^+$ -$X^1\Sigma^+$ and $D^1\Pi$-$X^1\Sigma^+$, and all TDMs have an extremum point around 5 Å, while the one of $C^1\Sigma^+$-$X^1\Sigma^+$ has a second extremum point at 7.8 Å.

The Franck-Condon factors (FCFs) of spontaneous radiative transitions are displayed in Table II, which describe the overlap of the vibrational wave functions for $A^1\Sigma^+$-$X^1\Sigma^+$, $C^1\Sigma^+$-$X^1\Sigma^+$, $B^1\Pi$-$X^1\Sigma^+$ and $D^1\Pi$-$X^1\Sigma^+$ transitions. All possible transitions between $0 \leqslant v' \leqslant 5$ and $0 \leqslant v'' \leqslant 5$ appear in the Table II, and, the $D^1\Pi$-$X^1\Sigma^+$ ones are the largest. The spontaneous radiative lifetimes are collected in Table III for selected vibrational states of the transitions from the four excited states in the lower vibrational levels to the ground state $X^1\Sigma^+$. Compared to $C^1\Sigma^+$-$X^1\Sigma^+$ (251–270 ns), the lifetimes of $A^1\Sigma^+$-$X^1\Sigma^+$ (31.28–32.09 ns), $B^1\Pi$-$X^1\Sigma^+$ (18.45–19.82

TABLE III. Lifetimes (ns) for $Z\,(v', J'=0)$ - $X^1\Sigma^+\,(v'', J''=0)$ ($Z = A^1\Sigma^+, C^1\Sigma^+, B^1\Pi, D^1\Pi$).

	$v'=0$	$v'=1$	$v'=2$	$v'=3$	$v'=4$
$A^1\Sigma^+$-$X^1\Sigma^+$	31.28	31.44	31.58	31.74	32.09
$C^1\Sigma^+$-$X^1\Sigma^+$	251.00	256.00	264.00	264.00	270.00
$B^1\Pi$-$X^1\Sigma^+$	18.45	18.77	19.45	19.45	19.82
$D^1\Pi$-$X^1\Sigma^+$	28.50	28.36	28.36	28.36	28.35

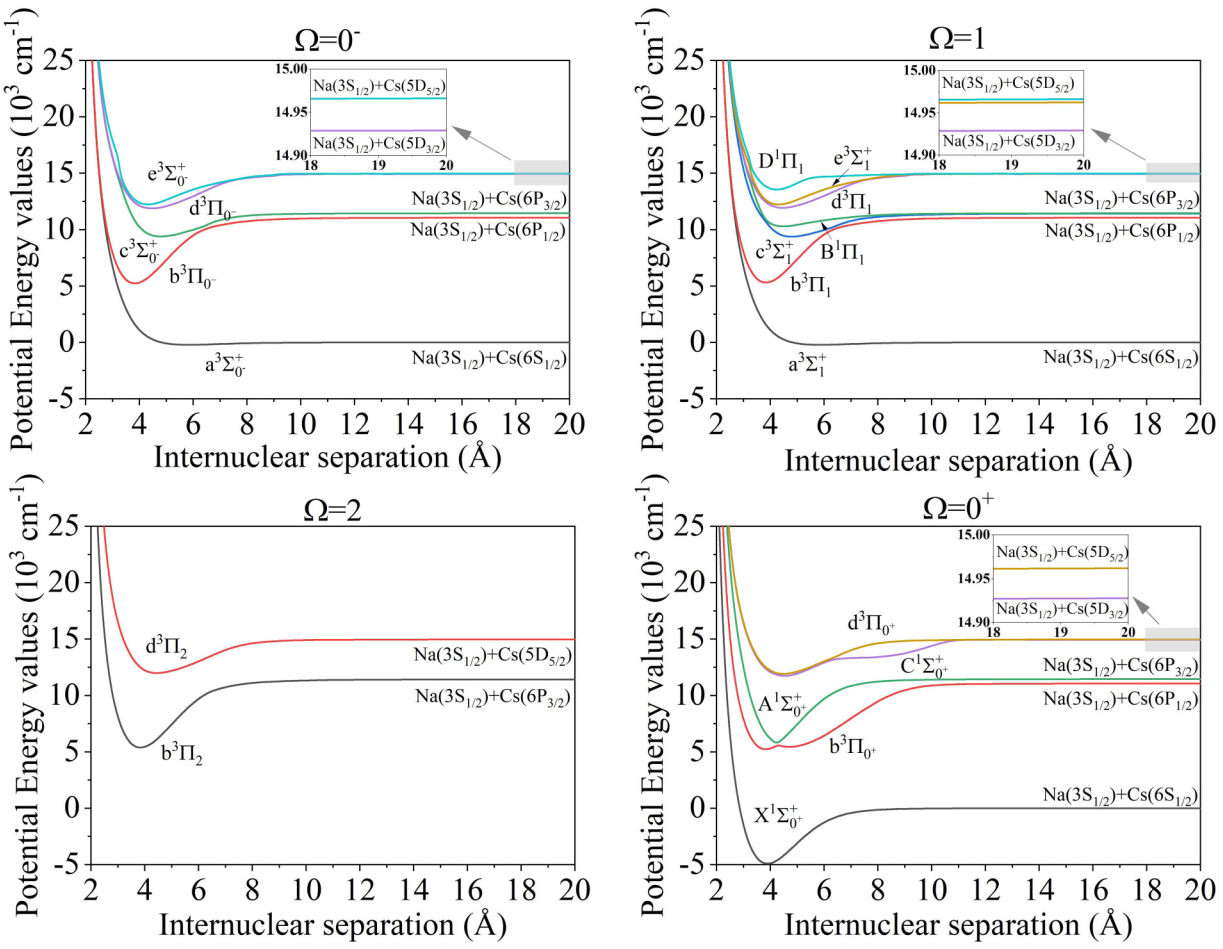

FIG. 4. Calculated MRCI + Q PECs of Ω states of NaCs molecule.

ns), and $D^1\Pi$-$X^1\Sigma^+$ (28.5–28.35 ns) are smaller, which fact facilitates rapid laser cooling. This is useful for the preparation of ultracold ground state NaCs molecules by PA. More information is given in Tables S3–S7.

C. PECs and spectroscopic constants of Ω states

The SOC effect has an important influence in the study of electronic structure of NaCs molecules. The PECs of Ω states are displayed in Fig. 4, and classified according to $\Omega = 0^+$, 0^-, 1, 2. The 10 electronic states in the first three dissociation limits of the Λ-S state basis split into 19 Ω states at five asymptotes, which consist of five $\Omega = 0^+$, five $\Omega = 0^-$, seven $\Omega = 1$ and two $\Omega = 2$. The asymptote of $\mathrm{Na}(3S_{1/2}) + \mathrm{Cs}(6S_{1/2})$ contains $X^1\Sigma^+_{0^+}$, $a^3\Sigma^+_1$ and $a^3\Sigma^+_{0^-}$; $\mathrm{Na}(3S_{1/2}) + \mathrm{Cs}(6P_{1/2})$ contains $b^3\Pi^+_0$, $b^3\Pi^-_0$ and $b^3\Pi_1$; $\mathrm{Na}(3S_{1/2}) + \mathrm{Cs}(6P_{3/2})$ contains $b^3\Pi_2$, $A^1\Sigma^+_{0^+}$, $c^3\Sigma^+_1$, $B^1\Pi_1$ and $c^3\Sigma^+_{0^-}$; $\mathrm{Na}(3S_{1/2}) + \mathrm{Cs}(5D_{3/2})$ contains $C^1\Sigma^+_{0^+}$, $d^3\Pi_{0^-}$ and $d^3\Pi_1$; $\mathrm{Na}(3S_{1/2}) + \mathrm{Cs}(5D_{5/2})$ contains $d^3\Pi_{0^+}$, $e^3\Sigma^+_{0^-}$, $d^3\Pi_2$, $e^3\Sigma^+_1$ and $D^1\Pi_1$.

According to Fig. 4 (see the shaded regions), the predicted dissociation limit undergoes a split after accounting for spin-orbit coupling effects, the differences are δE $(3s^2S_{1/2} + 6p^2P_{3/2} \rightarrow 3p^2P_{3/2} + 6s^2S_{1/2}) = 363\,\mathrm{cm}^{-1}$ and δE $(3s^2S_{1/2} + 5d^2D_{3/2} \rightarrow 3p^2P_{3/2} + 5d^2D_{5/2}) = 37\,\mathrm{cm}^{-1}$, respectively. This point is consistent with the experimental results. Avoided crossings are found at near 4 Å between $c^3\Sigma^+_1$ and $B^1\Pi_1$ for $\Omega = 1$ and between $A^1\Sigma^+_{0^+}$ and $b^3\Pi_{0^+}$ for $\Omega = 0^+$, therefore the $b^3\Pi_{0^+}$ state exhibits a double potential well. These avoided crossings can cause abrupt changes in the electronic wave functions of the relevant electronic states here.

The spectroscopic constants of Ω states are shown in Table IV. Comparing the calculations of nonempirical pseudopotentials by M. Korek *et al.* [21], the shorter bond lengths for Ω states are obtained and the differences ranges of R_e are within 0.07-0.33 Å. The discrepancies of T_e, ω_e, and B_e are within 39–259 cm^{-1}, 1.7−7.0 cm^{-1} (except $b^3\Pi \sim 17.6\,\mathrm{cm}^{-1}$ and $d^3\Pi \sim 12.0\,\mathrm{cm}^{-1}$), and 0.002−0.005 cm^{-1}, respectively. Larger deviations of T_e for $c^3\Sigma^+_1$ and $c^3\Sigma^+_{0^-}$ are just 2.82% and 2.73%. The results of our MRCI + ECP-spin-orbit operators (LS) comply with the existing theoretical calculations.

The trend of the potential energy profile of the Ω states is essentially unchanged compared to the Λ-S states, despite the presence of the avoided crossings. Examining carefully the spectroscopic constants without (Table I) and with the SOC (Table IV) of NaCs, the effect of the SOC on the spectroscopic properties is weak. The spectroscopic constants change only slightly (for ground state $X^1\Sigma^+$ and $X^1\Sigma^+_{0^+}$, $\delta R_e = 0.0014$ Å, $\delta T_e = 5.81\,\mathrm{cm}^{-1}$, $\delta\omega_e = 0.42\,\mathrm{cm}^{-1}$, $\delta\omega_e x_e = 0.018\,\mathrm{cm}^{-1}$, $\delta B_e = 0.00\,\mathrm{cm}^{-1}$; for excited states, $\delta R_e =$

TABLE IV. Spectroscopic Constants of Ω states of the NaCs Molecule.

	State	R_e (Å)	T_e (cm^{-1})	ω_e (cm^{-1})	$\omega_e x_e$ (cm^{-1})	B_e (cm^{-1})	Ref.
0^+	$X^1\Sigma^+$	3.890	0	97.77	0.334	0.0569	This work
		3.769	0	101.90		0.0605	CI [21]
	$b^3\Pi$	3.829	10136	78.98	2.997	0.0587	This work
		3.702	10151	96.60		0.0627	CI [21]
	$A^1\Sigma^+$	4.233	10713	158.84	3.351	0.0479	This work
		4.162	10962				CI [21]
	$C^1\Sigma^+$	4.522	16642	62.67	0.314	0.0421	This work
		4.421	16644				CI [21]
	$D^3\Pi$	4.470	16825	58.85	0.266	0.043	This work
		4.390	16865				CI [21]
0^-	$a^3\Sigma^+$	5.849	4696	19.83	0.442	0.0251	This work
		5.515	4954	21.80		0.0282	CI [21]
	$b^3\Pi$	3.827	10142	95.84	0.237	0.0587	This work
		3.695	10167	100.40		0.0629	CI [21]
	$c^3\Sigma^+$	4.794	14297	52.82	0.296	0.0374	This work
		4.537	14687	57.70		0.0417	CI [21]
	$D^3\Pi$	4.446	16791	56.65	0.254	0.0435	This work
		4.206	16700	111.30		0.1114	CI [21]
	$e^3\Sigma^+$	4.308	17137	68.36	0.441	0.0464	This work
		4.234	17019	69.71		0.0479	CI [21]
1	$a^3\Sigma^+$	5.849	4696	19.83	0.442	0.0251	This work
		5.516	4955	21.69		0.0282	CI [21]
	$b^3\Pi$	3.831	10214	95.78	0.235	0.0586	This work
		3.689	10254	100.62		0.0631	CI [21]
	$c^3\Sigma^+$	4.794	14285	52.53	0.307	0.0374	This work
		4.537	14687	57.40		0.0417	CI [21]
	$B^1\Pi$	4.478	15199	52.09	0.721	0.0429	This work
		4.290	15430	59.08		0.0467	CI [21]
	$D^3\Pi$	4.447	16845	56.56	0.268	0.0435	This work
		4.300	16794	68.54		0.0465	CI [21]
	$e^3\Sigma^+$	4.306	17135	68.39	0.441	0.0464	This work
		4.217	17095	64.91		0.0485	CI [21]
	$D^1\Pi$	4.235	18462	72.56	0.451	0.048	This work
2	$b^3\Pi$	3.836	10287	95.74	0.233	0.0585	This work
		3.682	10345	101.25		0.0634	CI [21]
	$D^3\Pi$	4.450	16895	56.53	0.282	0.0434	This work
		4.326	16942	58.24		0.0459	CI [21]

0.00−0.06 Å, $\delta T_e = 5 - -83\,\text{cm}^{-1}$, $\delta\omega_e = 0.01-2.34\,\text{cm}^{-1}$, $\delta\omega_e x_e = 0.00-3.31\,\text{cm}^{-1}$, $\delta B_e = 0.00-0.01\,\text{cm}^{-1}$; but, for $A^1\Sigma^+_{0^+}$ $\delta R_e = 0.50$ Å, $\delta\omega_e = 102.0\,\text{cm}^{-1}$ and for $b^3\Pi^+_0$ $\delta\omega_e = 17.45\,\text{cm}^{-1}$). The results of these calculations show that the use of ECP to calculate the SO effect has no significant effect on the spectroscopic constants. Nevertheless, the overall SOC effects play an important role in the electronic structure study of NaCs molecules.

The information about the asymptotes is presented in Table V, which contains the numbers of Ω states and the energies at the asymptotes. Compared with the experimental results, the accuracy of our calculation (error range

TABLE V. Number of Ω states and asymptotic information.

Na	Cs	Ω	E_{exp} (cm^{-1})	$(E_{\text{exp}} - E_{\text{cal}})/E_{\text{exp}}(\%)$ [CI]	E_{cal} (cm^{-1})	$(E_{\text{exp}} - E_{\text{cal}})/E_{\text{exp}}(\%)$ [MRCI]
$3s^2S_{1/2}$	$6s^2S_{1/2}$	$\Omega = 0^+, 0^-, 1$	0	0	0	0
$3s^2S_{1/2}$	$6p^2P_{1/2}$	$\Omega = 0^+, 0^-, 1$	11178	1.6	11061	0.01
$3s^2S_{1/2}$	$6p^2P_{3/2}$	$\Omega = 0^+, 0^-, 1, 1, 2$	11732	0.04	11424	0.026
$3s^2S_{1/2}$	$5d^2D_{3/2}$	$\Omega = 0^+, 0^-, 1, 1, 1, 2, 2, 3$	14499	0.14	14929	0.029
$3s^2S_{1/2}$	$5d^2D_{5/2}$	$\Omega = 0^+, 0^-, 1, 1, 2$	14597	0.26	14966	0.025
$3p^2P_{1/2}$	$6s^2S_{1/2}$	$\Omega = 0^+, 0^-, 1$	16956	0.17	16551	0.024
$3p^2P_{3/2}$	$6s^2S_{1/2}$	$\Omega = 0^+, 0^-, 1, 1, 2$	16973	0.03	16587	0.023

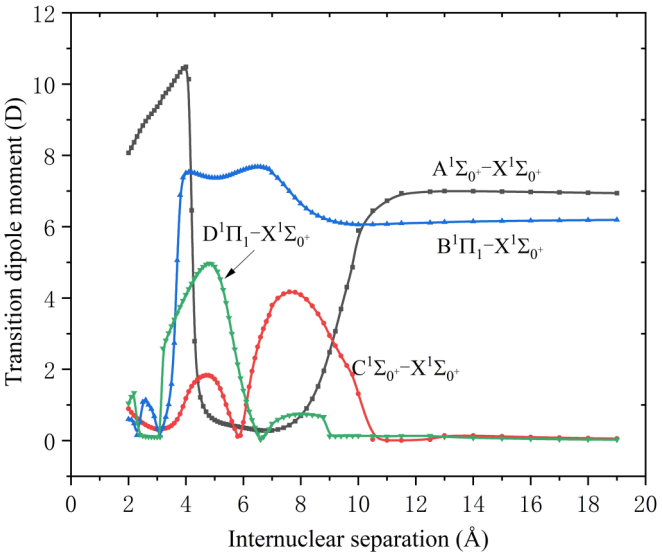

FIG. 5. TDMs of $A^1\Sigma^+_{0^+}$, $C^1\Sigma^+_{0^+}$, $B^1\Pi_1$, $D^1\Pi_1$ to $X^1\Sigma^+_{0^+}$.

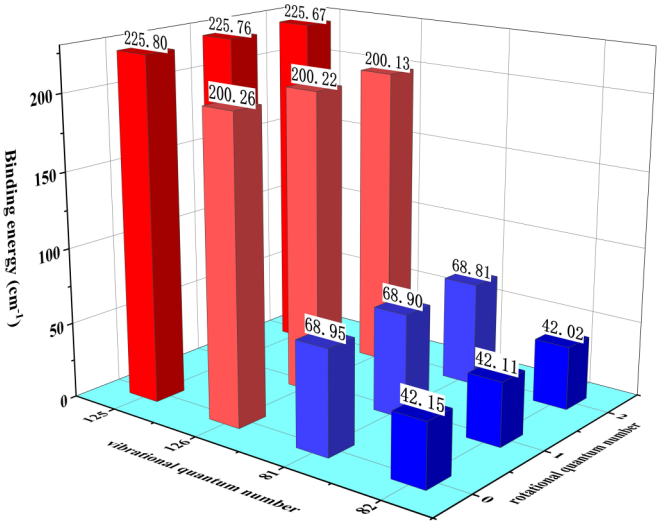

FIG. 6. Comparison of the binding energies of the theoretically calculated and experimental $b^3\Pi^+_0$ states. The red part is the theoretically calculated binding energy of $v' = 125, 126$. The blue part is the binding energy of $v' = 81, 82$ in the experiment.

0.01%−0.03%, and a more stable deviation ∼0.025% in the range of two asymptotes $3s^2S_{1/2} + 6p^2P_{3/2}$ and $3p^2P_{3/2} + 6s^2S_{1/2}$) are significantly better than that of the calculation of Korek *et al.* [21].

D. Transition properties and radiative lifetimes of Ω states

According to Eqs. (1) and (2), the radiation lifetimes of the Ω states were calculated. The TDMs of the $A^1\Sigma^+_{0^+}$-$X^1\Sigma^+_{0^+}$, $C^1\Sigma^+_{0^+}$-$X^1\Sigma^+_{0^+}$, $B^1\Pi_1$-$X^1\Sigma^+_{0^+}$, and $D^1\Pi_1$-$X^1\Sigma^+_{0^+}$ states are shown in Fig. 5. The TDMs of other $\Omega = 1$ to $\Omega = 0^+$ are displayed in Table S8. The FCFs of Ω states are displayed in Table S9. Comparing Figs. 3 and 5, we see that the TDMs of $A^1\Sigma^+_{0^+}$-$X^1\Sigma^+_{0^+}$ and $B^1\Pi_1$-$X^1\Sigma^+_{0^+}$ are noticeably smaller than $A^1\Sigma^+$-$X^1\Sigma^+$ and $B^1\Pi$-$X^1\Sigma^+$. Meanwhile, $B^1\Pi_1$-$X^1\Sigma^+_{0^+}$ shows a more pronounced variation at 4–10 Å, this may be caused by the same mechanism as the avoiding crossing in the vicinity of 4 Å.

The lifetimes for Z-$X^1\Sigma^+_{0^+}$ ($Z = A^1\Sigma^+_{0^+}$, $C^1\Sigma^+_{0^+}$, $B^1\Pi_1$, $D^1\Pi_1$) are displayed in Table VI and Tables S10-S13. The radiative lifetime of $\Omega = 1$ to $\Omega = 0^+$ are listed in Tables S12-S18. By comparing Table III and Table VI, it can be found that the radiation lifetimes of $A^1\Sigma^+$-$X^1\Sigma^+$, $B^1\Pi$ $B^1\Pi$-$X^1\Sigma^+$, $B^1\Pi$-$X^1\Sigma^+$ and $D^1\Pi$-$X^1\Sigma^+$ are not almost changed at all with and without considering the spin-orbit coupling effect.

The binding energies of the $b^3\Pi^+_0$ state was calculated and compared with the previous experiments [57,58]. The corresponding results are depicted in Fig. 6. As can be seen, the difference between any two adjacent red cuboids ($v' = 125$, 126) is almost the same as the difference between the adjacent blue cuboids ($v' = 81$, 82) at the corresponding position.

TABLE VI. Lifetimes (ns) for Z-$X^1\Sigma^+_{0^+}$ ($Z = A^1\Sigma^+_{0^+}$, $C^1\Sigma^+_{0^+}$, $B^1\Pi_1$, $D^1\Pi_1$).

	$v' = 0$	$v' = 1$	$v' = 2$	$v' = 3$	$v' = 4$
$A^1\Sigma^+_{0^+}$-$X^1\Sigma^+_{0^+}$	35.78	39.12	41.92	41.92	42.24
$C^1\Sigma^+_{0^+}$-$X^1\Sigma^+_{0^+}$	271.84	301.45	301.45	301.45	314.12
$B^1\Pi_1$-$X^1\Sigma^+_{0^+}$	18.83	19.19	19.96	19.96	20.39
$D^1\Pi_1$-$X^1\Sigma^+_{0^+}$	28.54	28.48	28.40	28.40	28.39

E. Proposed laser frequencies for the preparation of the ultracold ground-state NaCs molecules by the STIRAP method

In our previous work [31], the NaCs molecules in the excited state at the Na(3S) + Cs(6P) asymptote were obtained using PA. After the calculation of the energy levels of the bound states of the $b^3\Pi$ and $A^1\Sigma^+$ electronic states, it was found that there was a large overlap of wave functions, which would cause a strong coupling between the $b^3\Pi$ and $A^1\Sigma^+$ states, resulting in losses and affecting the process of spontaneous radiation.

Under the action of SOC, the $b^3\Pi$ state splits into $b^3\Pi^+_0$, $b^3\Pi^-_0$, $b^3\Pi_1$, and $b^3\Pi_2$ states. The large number of transitions available between ground singlet and ground triplet and A-b mixed levels, and the Frank-Condon factor mapping does not overlap well between $B^1\Pi$ and deeply bound ground singlet. If we use the higher excited state $D^1\Pi$, the bigger FCFs comparing with $B^1\Pi$ can been found in Table II. This means that the overlaps of the wave functions between the ground and excited states are better, thus making the transition easier to achieve.

STIRAP technique has the characteristics of low loss and higher preparation efficiency to create the molecules at the rovibrational ground state. The scheme can be understood as a coherent two-photon Raman transition in a three-level system, which is usually applied to realize a population transfer between two quantum states that have large energy gaps. In the STIRAP scheme, three energy states are involved, the initial state $|i\rangle$, the intermediate (excited) state $|e\rangle$, and the final (ground) state $|g\rangle$.

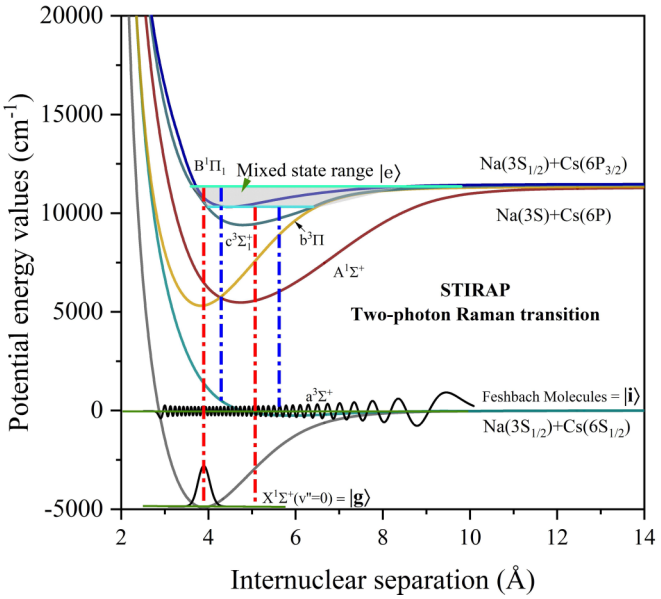

FIG. 7. Diagram of the NaCs electronic ground and excited molecular-state potentials and the vibrational levels involved in the two-photon coherent state transfer to the singlet ground state. Here, the intermediate state $|e\rangle$ is the mixed state of $B^1\Pi_1$ and $c^3\Sigma_1^+$, while the initial state $|i\rangle$ is a weakly bound Feshbach molecule and the final state $|g\rangle$ is the rovibrational ground state ($v = 0$, $J = 0$). The red dashed lines are laser ω_1, the blue dashed lines are laser ω_2.

The STIRAP process of NaCs molecules is shown in Fig. 7, the lowest rovibrational state ($v = 0$, $J = 0$) of the ground state is the final state to be prepared, the first asymptote Na($3s$) + Cs($6s$) of the NaCs molecule is an initial state. The purpose of this choice is to form a dark state between the two ground states during the preparation process so as to ignore the influence of the excited state. In the choice of intermediate state, we follow the two rules: The intermediate state has favorable transition dipole moments for both the up leg ($|i\rangle$ to $|e\rangle$) and the down leg ($|e\rangle$ to $|g\rangle$). On the other hand, the initial Feshbach molecular state is a blend of a singlet and a triplet state, according to the transition selection rule, in which the intermediate state must feature strong singlet-triplet mixing and the energy levels of the two potential energy curves must have enough overlap. In this case, the intermediate state can strongly connect the initial Feshbach molecular state to the absolute rovibrational singlet ground state.

Large TDMs mean that the Franck-Condon overlap between the two states where the transition occurs is significant. The results in Figs. 3 and 5 showed that the $c^3\Sigma^+$ and $B^1\Pi$ states have large TDMs near 4 Å and at 10–20 Å, independently of the SOC effect. Therefore, we have chosen the [$c^3\Sigma^+$-$B^1\Pi$] system as the selection range of the intermediate state. Since the intermediate state is deeply bound, the change caused by the numerical method and BSSE is not large enough to make a modification to the deeply bound vibrational state number.

All energy positions of vibrational levels of the $c^3\Sigma^+/c^3\Sigma^+{}_1$ and $B^1\Pi/B^1\Pi_1$ states were calculated and displayed in Table VII. The calculation results show that the $v' = 0$ (10334.5132 cm^{-1}) vibrational level of the $B^1\Pi$ state is close to the $v' = 19$ (10325.1268 cm^{-1}) vibrational level

TABLE VII. Vibrational term values $T_{v'}$ (cm^{-1}) with $J = 0$ of the $c^3\Sigma^+$, $c^3\Sigma_1^+$, $B^1\Pi$ and $B^1\Pi_1$. The $c^3\Sigma_1^+$ and $B^1\Pi_1$ denotes the states with SOC that populated below the NaCs first dissociation limit $3S_{1/2} + 6P_{1/2}$.

v'	$c^3\Sigma_1^+$ $T_{v'}$	$c^3\Sigma^+$ $T_{v'}$	$B^1\Pi_1$ $T_{v'}$	$B^1\Pi$ $T_{v'}$
0	9401.2165	9479.8955	**10314.9261**	**10334.5132**
1	9453.2495	9532.5697	10365.7349	10384.2366
2	9504.6178	9584.2527	10415.0365	10432.4777
3	9555.3221	9634.9249	10462.8285	10479.2258
4	9605.3662	9684.5753	10509.1155	10524.4838
5	9654.761	9733.1965	10553.9096	10568.268
6	9703.5218	9780.8018	10597.2333	10610.5878
7	9751.6686	9827.418	10639.1199	10651.4644
8	9799.2293	9873.0927	10679.6111	10690.9211
9	9846.242	9917.887	10718.7524	10728.9808
10	9892.7559	9961.856	10756.5894	10765.6692
11	9938.8333	10005.0482	10793.1651	10801.0182
12	9984.5501	10047.4988	10828.5198	10835.0595
13	10029.9923	10089.2321	10862.6917	10867.8248
14	10075.2496	10130.2624	10895.718	10899.3485
15	10120.4042	10170.6003	10927.6353	10929.6631
16	10165.5183	10210.2531	10958.4794	10958.7972
17	10210.6215	10249.2248	10988.286	10986.7655
18	10255.7089	10287.5152	11017.0891	11013.5806
19	**10300.7444**	**10325.1268**	11044.922	11039.2527
20	10345.6622	10362.0613	11071.8167	11063.7852
21	10390.3813	10398.3186	11097.8033	11087.1795
22	10434.814	10433.8993	11122.9074	11109.4392
23	10478.8666	10468.8047	11147.15	11130.5806
24	10522.4474	10503.0371	11170.5443	**11150.6152**
25	10565.4673	10536.5989	11193.0957	11169.5471
26	10607.8409	10569.4959	11214.8004	11187.3743
27	10649.4824	10601.7301	11235.6442	11204.0896
28	10690.321	10633.2999	11255.6036	11219.6843
29	10730.2749	10664.2031	11274.6462	11234.1621
30	10769.2823	10694.4292	11292.7331	11247.5314
31	10807.2733	10723.9587	11309.8215	11259.8025
32	10844.1853	10752.771	**11325.8672**	11271.0061
33	10879.9606	10780.8497	11340.8283	11281.169
34	10914.5376	10808.1788	11354.6751	11290.3055
35	10947.8684	10834.7422	11367.4098	11298.9554
36	10979.8993	10860.5346	11379.0701	
37	11010.5941	10885.5503	11389.545	
38	11039.9212	10909.7814	11398.8019	
39	11067.8588	10933.2252		
40	11094.4002	10955.8775		
41	11119.548	10977.7342		
42	11143.3181	10998.8		
43	11165.7396	11019.0738		
44	11186.8464	11038.5564		
45	11206.6837	11057.2491		
46	11225.2963	11075.1581		
47	11242.7487	11092.2887		
48	11259.181	11108.643		
49	11274.9184	11124.2038		
50	11290.12	11138.9343		
51	11304.1023	**11152.9395**		
52	11316.5873			
53	**11328.7056**			

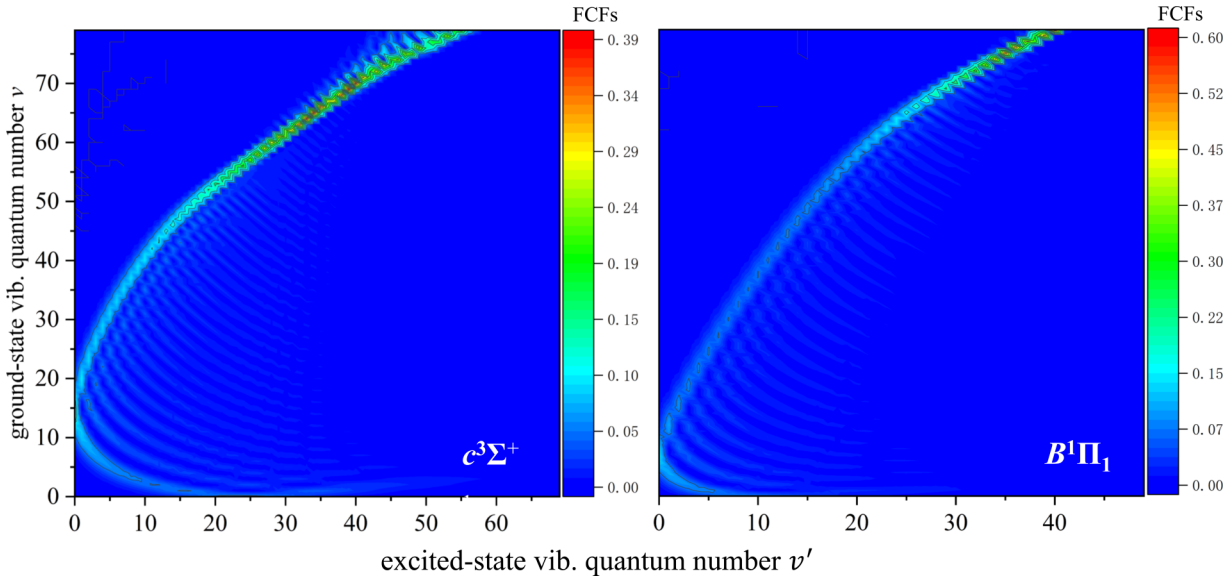

FIG. 8. Effective Franck-Condon factors calculated for transitions between intermediate and ground states NaCs molecule. The transition FCFs of the two excited states to the ground state reach 0.4 and 0.6, respectively. It is a very attractive condition in the experiment.

of the $c^3\Sigma^+$ state and the $v' = 24$ (11150.6152 cm^{-1}) vibrational level of the $B^1\Pi$ state is close to the $v' = 51$ (11152.9395 cm^{-1}) vibrational level of the $c^3\Sigma^+$ state. So far, the probable mixing ranges as $v' = 0$–24 of $B^1\Pi$ state and $v' = 19$–51 of $c^3\Sigma^+$ state have been obtained by our theoretical calculation. Based on these energy values, the wavelength ranges of the two lasers for STIRAP are calculated as $\omega_1 = 622.8-656.7$ nm and $\omega_2 = 896.3-969.8$ nm. Using the same approach, the wavelength ranges of the laser are obtained through the mixed state of $c^3\Sigma_1^+$ and $B^1\Pi_1$ are 617.677–659.555 nm and 882.713–970.804 nm. In a recent experiment [59], Cairncross *et al.* has created a single ground state NaCs molecule through STIRAP via the $c^3\Sigma_1^+$ ($v' = 26$) excited state using two lasers with the wavelengths 635 and 922 nm.

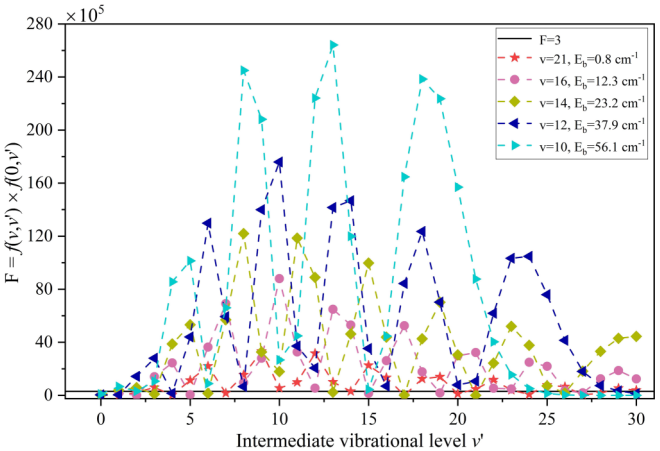

FIG. 9. Products of Franck-Condon factors describing the transition probabilities in STIRAP processes between a starting ground vibrational level v, an intermediate vibrational level v' in the excited electronic state and the rovibrational ground state. E_b is the binding energy.

The laser wavelengths used in the experiments are within the range of our theoretically calculated laser wavelengths.

In addition, to estimate the transfer efficiency, the transition properties of intermediate states to ground state are analyzed. And a function $F = f(v, v') \times f(0, v')$ is defined to characterize the transition efficiency of the STIRAP process, where f represents the FCF of the two transitions.

Diagonalized FCFs are necessary for the efficient preparation of ultracold molecules using the STIRAP scheme. As shown in Fig. 8, the FCFs for the transition of the A and B states to the ground state are calculated by us, and are highly diagonalized.

Based on the range of intermediate states determined before, we selected six vibrational ($v = 10$, 12, 14, 16, 19, 21) energy levels among them for the study of transition efficiency. Following a similar analysis of the RbSr system of Chen *et al.* [60], in Fig 9. the products of Franck-Condon factors for the two transitions between the initial ground vibrational states v and target rovibrational ground state as a function of the intermediate excited vibrational state v'.

As shown in Fig. 9, the F value range of the selected intermediate state is $2.38 \times 10^{-3} \sim 1.23 \times 10^{-8}$. The most value of F is over 3×10^{-5}. This indicates that this scheme satisfies the conditions for the efficient preparation of ultracold NaCs molecules that should have a large F value. Generally, the more deeply bound initial vibrational state v, the easier the STIRAP process will be. We find that it is in many cases possible to select an intermediate excited state where the product of the two relevant Franck-Condon factors is sufficient to achieve high STIRAP efficiencies.

IV. CONCLUSIONS

The high-precision PECs, spectroscopic constants, and transition properties of Λ-S states and Ω states have been calculated for the NaCs molecule. The calculated results comply with the existing earlier theoretical and experimental data.

The binding energy data is calculated, and verified with our previous experiment, the fine structures of $b^3\Pi_0^+$ ($v' = 81,82$) are predicted; The mixed states of $A^1\Sigma^+$ and $b^3\Pi$ are evaluated with PECs of Ω states, which contain $X^1\Sigma_{0^+}^+$, $b^3\Pi_0^+$, $b^3\Pi_0^-$, $b^3\Pi_1$, and $b^3\Pi_2$; The radiative transition from a higher $^1\Pi$ state to the ground state in the PA is discussed. New two-photon Raman transition channels are predicted, their corresponding laser wavelength ranges for the $B^1\Pi_1$ and $c^3\Sigma_1^+$ states are 617.677–659.555 nm and 882.713–970.804 nm in the STIRAP process and transition efficiency is evaluated. The results provide a promising theoretical reference for further experimental research on NaCs molecule.

ACKNOWLEDGMENTS

This work was supported by National Natural Science Foundation of China (NSFC) (Grants No. 11604187 and No 62175140), the Natural Science Young Foundation of Shanxi Province (Grant No. 201801D221004), Cooperation projects of Institute of Applied Physics and Computational Mathematics, Open Fund of Key Laboratory of Advanced Reactor Engineering and Safety, Ministry of Education (Tsinghua University, China), the collaborative grant of the Russian Foundation for Basic Research (RFBR) and National Natural Science Foundation of China (NSFC) (No. 20-53-53025 in the RFBR classification and No. 62011530047 in the NSFC classification).

[1] J. L. Bohn, A. M. Rey, and J. Ye, Cold molecules: Progress in quantum engineering of chemistry and quantum matter, Science **357**, 1002 (2017).

[2] K. R. Hazzard, B. Gadway, M. Foss-Feig, B. Yan, S. A. Moses, J. P. Covey, N. Y. Yao, M. D. Lukin, J. Ye, D. S. Jin, and A. M. Rey, Many-Body Dynamics of Dipolar Molecules in an Optical Lattice, Phys. Rev. Lett. **113**, 195302 (2014).

[3] R. V. Krems, W. C. Stwalley, and B. Friedrich, *Cold Molecules: Theory, Experiment, Applications* (CRC Press, Boca Raton, 2009).

[4] G. Pupillo, A. Griessner, A. Micheli, M. Ortner, D.-W. Wang, and P. Zoller, Cold Atoms and Molecules in Self-Assembled Dipolar Lattices, Phys. Rev. Lett. **100**, 050402 (2008).

[5] L. Bomble, P. Pellegrini, P. Ghesquiere, and M. Desouter-Lecomte, Toward scalable information processing with Ultracold polar molecules in an electric field: A numerical investigation, Phys. Rev. A **82**, 062323 (2010).

[6] P. D. Gregory, J. A. Blackmore, S. L. Bromley, J. M. Hutson, and S. L. Cornish, Robust storage qubits in Ultracold polar molecules, Nat. Phys. **17**, 1149 (2021).

[7] M. A. Baranov, M. Dalmonte, G. Pupillo, and P. Zoller, Condensed matter theory of dipolar quantum gases, Chem. Rev. **112**, 5012 (2012).

[8] J. Lin, J. He, M. Jin, G. Chen, and D. Wang, Seconds-Scale Coherence on Nuclear Spin Transitions of Ultracold Polar Molecules in 3D Optical Lattices, Phys. Rev. Lett. **128**, 223201 (2022).

[9] S. Ospelkaus, K.-K. Ni, M. De Miranda, B. Neyenhuis, D. Wang, S. Kotochigova, P. Julienne, D. Jin, and J. Ye, Ultracold polar molecules near quantum degeneracy, Faraday Discuss. **142**, 351 (2009).

[10] J. Pérez Ríos, *An Introduction to Cold and Ultracold Chemistry* (Springer, New York, 2020).

[11] S. Ospelkaus, K. K. Ni, D. Wang, M. H. G. de Miranda, B. Neyenhuis, G. Quéméner, P. S. Julienne, J. L. Bohn, D. S. Jin, and J. Ye, Quantum-state controlled chemical reactions of ultracold potassium-rubidium molecules, Science **327**, 853 (2010).

[12] M. Guo, B. Zhu, B. Lu, X. Ye, F. Wang, R. Vexiau, N. Bouloufa-Maafa, G. Quéméner, O. Dulieu, and D. Wang, Creation of an Ultracold gas of ground-state dipolar ^{23}Na ^{87}Rb molecules, Phys. Rev. Lett. **116**, 205303 (2016).

[13] H. Son, J. J. Park, W. Ketterle, and A. O. Jamison, Collisional cooling of Ultracold molecules, Nature (London) **580**, 197 (2020).

[14] H. Yang, D.-C. Zhang, L. Liu, Y.-X. Liu, J. Nan, B. Zhao, and J.-W. Pan, Observation of magnetically tunable feshbach resonances in Ultracold ^{23}Na ^{40}K + ^{40}K collisions, Science **363**, 261 (2019).

[15] B. Yan, S. A. Moses, B. Gadway, J. P. Covey, K. R. A. Hazzard, A. M. Rey, D. S. Jin, and J. Ye, Observation of dipolar spin-exchange interactions with lattice-confined polar molecules, Nature (London) **501**, 7468 (2013).

[16] C. E. Faust, Ph.D. thesis, Experimental studies of interacting electronic states in NaCs, Lehigh University, 2014.

[17] P. S. Żuchowski and J. M. Hutson, Reactions of Ultracold alkali-metal dimers, Phys. Rev. A **81**, 060703(R) (2010).

[18] G. Igel-Mann, U. Wedig, P. Fuentealba, and H. Stoll, Ground-state properties of alkali dimers XY ($X, Y = Li$ to Cs), J. Chem. Phys. **84**, 5007 (1986).

[19] M. Korek, A.-R. Allouche, K. Fakhreddine, and A. Chaalan, Theoretical study of the electronic structure of LiCs, NaCs, and KCs molecules, Can. J. Phys. **78**, 977 (2000).

[20] M. Aymar and O. Dulieu, Calculation of accurate permanent dipole moments of the lowest $^{1,3}\Sigma^+$ states of heteronuclear alkali dimers using extended basis sets, J. Chem. Phys. **122**, 204302 (2005).

[21] M. Korek, S. Bleik, and A.-R. Allouche, Theoretical calculation of the low laying electronic states of the molecule nacs with spin-orbit effect, J. Chem. Phys. **126**, 124313 (2007).

[22] R. Dardouri, K. Issa, B. Oujia, and F. Xavier Gadéa, Theoretical study of the electronic structure of LiX and NaX (X = Rb, Cs) molecules, Int. J. Quantum Chem. **112**, 2724 (2012).

[23] N. Mabrouk and H. Berriche, Theoretical study of the CsNa molecule: Adiabatic and diabatic potential energy and dipole moment, J. Phys. Chem. A **118**, 8828 (2014).

[24] U. Diemer, H. Weickenmeier, M. Wahl, and W. Demtröder, Sub-doppler spectroscopy of the nacs molecule, Chem. Phys. Lett. **104**, 489 (1984).

[25] O. Docenko, M. Tamanis, J. Zaharova, R. Ferber, A. Pashov, H. Knöckel, and E. Tiemann, The coupling of the $X^1\Sigma^+$ and $a^3\Sigma^+$ states of the atom pair Na + Cs and modelling cold collisions, J. Phys. B **39**, S929 (2006).

[26] O. Docenko, M. Tamanis, J. Zaharova, R. Ferber, and E. Tiemann, High resolution spectroscopy and potential determination of the $(3)^1\Pi$ state of nacs, J. Chem. Phys. **124**, 174310 (2006).

[27] C. Haimberger, J. Kleinert, O. Dulieu, and N. Bigelow, Processes in the formation of Ultracold nacs, J. Phys. B **39**, S957 (2006).

[28] J. Zaharova, M. Tamanis, R. Ferber, A. Drozdova, E. Pazyuk, and A. Stolyarov, Solution of the fully-mixed-state problem: Direct deperturbation analysis of the $A^1\Sigma^+$ -$b^3\Pi$ complex in a nacs dimer, Phys. Rev. A **79**, 012508 (2009).

[29] P. Zabawa, A. Wakim, A. Neukirch, C. Haimberger, N. Bigelow, A. Stolyarov, E. Pazyuk, M. Tamanis, and R. Ferber, Near-dissociation photoassociative production of deeply bound nacs molecules, Phys. Rev. A **82**, 040501(R) (2010).

[30] S. T. Ashman, Ph.D. thesis, Experimental studies of the sodium cesium 5 (3) Pi (0) and 1 (a) 3Sigma+ electronic states, Lehigh University, 2010.

[31] W. Liu, J. Wu, J. Ma, P. Li, V. B. Sovkov, L. Xiao, and S. Jia, Observation and analysis of the hyperfine structure of near-dissociation levels of the nacs $c^3\Sigma^+$ state below the dissociation limit $3S_{1/2} + 6P_{3/2}$,, Phys. Rev. A **94**, 032518 (2016).

[32] W. Liu, X. Wang, J. Wu, X. Su, S. Wang, V. B. Sovkov, J. Ma, L. Xiao, and S. Jia, Experimental observation and determination of the laser-induced frequency shift of hyperfine levels of Ultracold polar molecules, Phys. Rev. A **96**, 022504 (2017).

[33] K.-K. Ni, T. Rosenband, and D. D. Grimes, Dipolar exchange quantum logic gate with polar molecules, Chem. Sci. **9**, 6830 (2018).

[34] J. T. Zhang, Y. Yu, W. B. Cairncross, K. Wang, L. R. B. Picard, J. D. Hood, Y.-W. Lin, J. M. Hutson, and K.-K. Ni, Forming a Single Molecule by Magnetoassociation in an Optical Tweezer, Phys. Rev. Lett. **124**, 253401 (2020).

[35] J. P. Shaffer, W. Chalupczak, and N. P. Bigelow, Trap loss in a two-species na-cs magneto-optical trap: intramultiplet mixing in heteronuclear Ultracold collisions, Phys. Rev. A **60**, R3365 (1999).

[36] C. Haimberger, J. Kleinert, M. Bhattacharya, and N. P. Bigelow, Formation and detection of Ultracold ground-state polar molecules, Phys. Rev. A **70**, 021402(R) (2004).

[37] C. Haimberger, J. Kleinert, P. Zabawa, A. Wakim, and N. Bigelow, Formation of Ultracold, highly polar $X^1\Sigma^+$ nacs molecules, New J. Phys. **11**, 055042 (2009).

[38] J. Zaharova, O. Docenko, M. Tamanis, R. Ferber, A. Pashov, H. Knöckel, and E. Tiemann, The $B^1\Pi$ state of NaCs: high resolution laser induced fluorescence spectroscopy and potential construction, J. Chem. Phys. **127**, 224302 (2007).

[39] S. Ashman, B. McGeehan, C. Wolfe, C. Faust, K. Richter, J. Jones, A. Hickman, and J. Huennekens, Experimental studies of the nacs $5^3\Pi_0$ and $1(a)^3\Sigma^+$ states, J. Chem. Phys. **136**, 114313 (2012).

[40] P. Zabawa, A. Wakim, A. Neukirch, N. Bigelow, E. Pazyuk, A. Stolyarov, M. Tamanis, and R. Ferber, in 41st *APS Division of Atomic, Molecular and Optical Physics Meeting Abstracts* (American Physical Society, Houston, Texas, 2010), Vol. 55, p. OPB. 20.

[41] P. Zabawa, A. Wakim, M. Haruza, and N. Bigelow, Formation of Ultracold $X^1\Sigma^+$ ($v'' = 0$) nacs molecules via coupled photoassociation channels, Phys. Rev. A **84**, 061401(R) (2011).

[42] C. Faust, J. Jones, J. Huennekens, and R. Field, Experimental studies of the nacs $12(0^+)$ $[7^1\Sigma^+]$ state: Spin-orbit and nonadiabatic interactions and quantum interference in the $12(0^+)$ $[7^1\Sigma^+]$ and $11(0^+)$ $[5^3\Pi_0]$ emission spectra, J. Chem. Phys. **146**, 104302 (2017).

[43] L. Liu, J. Hood, Y. Yu, J. Zhang, N. Hutzler, T. Rosenband, and K.-K. Ni, Building one molecule from a reservoir of two atoms, Science **360**, 900 (2018).

[44] X. Wang, W. Liu, J. Wu, V. B. Sovkov, J. Ma, P. Li, L. Xiao, and S. Jia, Saturation of photoassociation in nacs dark magneto-optical trap, J. Quant. Spectrosc. Radiat. Trans. **240**, 106678 (2020).

[45] W. Wang, W. Liu, J. Wu, Y. Li, X. Wang, Y. Liu, J. Ma, L. Xiao, and S. Jia, Enhancement of signal-to-noise ratio of Ultracold polar nacs molecular spectra by phase locking detection, Chin. Phys. B **26**, 123701 (2017).

[46] H. J. Werner and P. J. Knowles, A second order multiconfiguration SCF procedure with optimum convergence, J. Chem. Phys. **82**, 5053 (1985).

[47] P. J. Knowles and H.-J. Werner, An efficient second-order MC SCF method for long configuration expansions, Chem. Phys. Lett. **115**, 259 (1985).

[48] H. J. Werner and P. J. Knowles, An efficient internally contracted multiconfiguration–reference configuration interaction method, J. Chem. Phys. **89**, 5803 (1988).

[49] P. J. Knowles and H.-J. Werner, An efficient method for the evaluation of coupling coefficients in configuration interaction calculations, Chem. Phys. Lett. **145**, 514 (1988).

[50] K. Shamasundar, G. Knizia, and H.-J. Werner, A new internally contracted multi-reference configuration interaction method, J. Chem. Phys. **135**, 054101 (2011).

[51] K. L. Schuchardt, B. T. Didier, T. Elsethagen, L. Sun, V. Gurumoorthi, J. Chase, J. Li, and T. L. Windus, Basis set exchange: A community database for computational sciences, J. Chem. Inf. Model. **47**, 1045 (2007).

[52] See Supplemental Material at http://link.aps.org/supplemental/10.1103/PhysRevA.105.063322 for detailed information on electronic state transitions of NaCs molecules.

[53] A. Berning, M. Schweizer, H.-J. Werner, P. J. Knowles, and P. Palmieri, Spin-orbit matrix elements for internally contracted multireference configuration interaction wavefunctions, Mol. Phys. **98**, 1823 (2000).

[54] H. J. Werner, P. J. Knowles, G. Knizia, F. R. Manby, and M. Schütz, And Wiley Interdisciplinary Reviews: Molpro: A general-purpose quantum chemistry program package, Computational Mol. Sci. **2**, 242 (2012).

[55] MOLPRO, version 2015.1, a package of *ab initio* programs, H.-J. Werner, P. J. Knowles, G. Knizia, F. R. Manby, and M. SchÜtz, and others, see http://www.molpro.net.

[56] R. J. Le Roy, LEVEL: A computer program for solving the radial schrödinger equation for bound and quasi-bound levels, J. Quant. Spectrosc. Radiat. Transfer **186**, 167 (2017).

[57] X. Wang, W. Liu, Y. Li, J. Wu, V. B. Sovkov, J. Ma, S. Onishchenko, P. Li, Y. Fu, and D. Li, Hyperfine structure of the nacs $b^3\Pi_2$ state near the dissociation limit $3S_{1/2} + 6P_{3/2}$ observed with Ultracold atomic photoassociation, Phys. Chem. Chem. Phys. **22**, 3809 (2020).

[58] P. J. Zabawa, Ph.D. thesis, Production of Ultracold, absolute vibrational ground state NaCs molecules, University of Rochester, 2012.

[59] W. B. Cairncross, J. T. Zhang, L. R. B. Picard, Y. Yu, K. Wang, and K.-K. Ni, Assembly of a Rovibrational Ground State Molecule in an Optical Tweezer, Phys. Rev. Lett. **126**, 123402 (2021).

[60] T. Chen, S. Zhu, X. Li, J. Qian, and Y. Wang, Optical Feshbach resonances and ground-state-molecule production in the rbhg system, Phys. Rev. A **89**, 063402 (2014).